OVERVIEW OF PLASMA EDGE PHYSICS

Bernhard Unterberg and Ulrich Samm Institut für Plasmaphysik, Forschungszentrum Jülich GmbH*, Association EURATOM-FZ Jülich D-52425 Jülich, Germany, phone: +49 2461 61 4803, email: B.Unterberg@fz-juelich.de

ABSTRACT

Basic properties of the plasma edge in magnetically confined fusion plasmas are summarised. Starting from the magnetic topology of tokamaks we describe the transport of the scrape-off layer including drifts and the consequences of the electrostatic Debye sheath in front of the plasma facing components. The relation between the local plasma density and temperature at the targets and the fluxes of power and particles in the SOL is discussed. The transport of the fuel neutrals (hydrogen atoms and molecules) is described.

I. INTRODUCTION

Processes at the edge plasma in general and plasma-wall interaction in particular play a crucial role for achieving a steady state burning fusion plasma. The first wall has to withstand and exhaust the α - particle heating power and the helium-ash must be removed (pumped) from the plasma. Wall erosion affects the lifetime of wall elements and releases impurities into the plasma, which then cause fuel dilution and energy loss due to radiation from the plasma centre. Moreover, also global confinement properties can be affected by edge processes. Therefore, understanding these processes and controlling the edge plasma by appropriate means is an important field of research.

The plasma in a tokamak or stellarator represents an open system. The wall is a perfect plasma sink and owing to the finite confinement times (energy and particle confinement times τ_E and τ_P) the plasma has to be renewed continuously. The energy content E is sustained by heating, $E = P_{heat} * \tau_E$, with the heating power P_{heat} . The number N of particles in the plasma is sustained by a permanent flow of D/T gas from the wall elements into the plasma, $N = \Gamma * \tau_p$. The alpha particles with a power density of $P_{\alpha} = 0.15 MW/m^3$ (T=10 keV, $n = 10^{20} m^{-3}$) lead to an average wall load of some $100kW/m^2$, if we take into account a plasma

volume of roughly $1000m^3$ for self- sustained burn - a moderate value. However, energy exhaust becomes a problem, because the magnetic field directs the convected heat load on rather small wall areas. This can lead to peak loads which could damage the wall.

Another important issue of edge physics is impurity generation and impurity exhaust. Any impurities in the plasma centre lead to fuel dilution reducing the fusion power. Their concentration has to stay below a certain level. E.g. the concentration of the unavoidable helium, which is generated at a rate of $R_{He} = 10^{18} s^{-1} m^{-3}$, should not exceed significantly a value of about 10%. This condition is fulfilled when the characteristic time $\tau_{p,He}^*$ for helium removal is sufficiently low [4], [5]. The experimental values found for $\tau_{p,He}^*$ are much larger (factor 10 or more) than the global confinement time of helium demonstrating that helium is recycling at the wall more than 10 times before it is removed by the pumps. The presence of other impurities in the plasma depends on the choice of wall materials, erosion processes and edge plasma properties, like temperature, density and particle transport.

No unique definition exists for the term "plasma edge" or "plasma boundary". An important part of the edge plasma is the scrape-off layer (SOL) which is that region of the plasma where the magnetic field lines intersect wall elements. But significant processes occur also inside the confined plasma, like neutral particle penetration, ionization, charge exchange or impurity line radiation. These atomic processes have an impact on the properties of both, the edge plasma and the core plasma.

In this lecture plasma edge physics is introduced comprising the SOL as well as part of the confined plasma. The relevant processes are discussed following the transport cycle of the particles beginning with the boundary conditions which are given by the magnetic topology. Then the transport inside the SOL, the electrostatic sheath, the relation between plasma parameters close to the plasma facing components and fluxes into the SOL and, finally, the penetration of neutrals into the plasma follow. The important aspect of edge radiation by impurities will be discussed in a sep-

^{*}Partner in the Trilateral Euregio Cluster

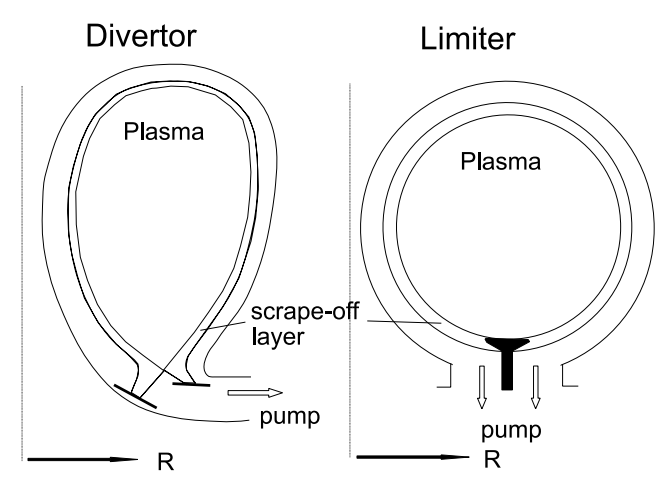


Figure 1: Poloidal divertor and toroidal limiter concept shown in the poloidal plane of a tokamak

arate lecture [1]. Overall, the physical processes in the plasma edge have important consequences for the interaction between plasma and wall and the resulting recycling and erosion mechanisms. This subject is discussed in [2].

An excellent introduction into the physics of the plasma boundary can be found in the book of P.C. Stangeby "The Plasma Boundary of Magnetic Fusion Devices" [3].

II. MAGNETIC TOPOLOGY

Wall elements which intersect the magnetic field serve as a perfect plasma sink and impose a flow directed along the field lines. The flux tubes generated at each wall element are filled with plasma by perpendicular transport (diffusion, drifts). This property helps to build up a particle density sufficient for helium exhaust. On the other hand the concentration of plasma flow on small areas is less beneficial for power exhaust, since a uniform plasma flow to the whole wall would avoid peak heat loads. The very details of particle and heat load on the wall are determined by the magnetic topology and the geometry of the plasma facing components. We have to distinguish two different concepts: divertor and limiter (cf. also [6]). The poloidal divertor shown in Fig. 1 is used in the performance oriented devices (JET, JT60-U, DIII-D, ASDEX-U) and is the preferred concept for the next step device. The simpler (and cheaper) limiter is explored e.g. in Tore Supra and TEXTOR (toroidal belt limiter), in particular, with respect to steady state technology, plasma-wall interaction and new concepts with ergodic boundaries.

The projection of the flux tubes on the surface of the limiter/divertor plate is determined by two angles: the tilting angle α between toroidal and poloidal direction depends on the rotational transform (safety factor)

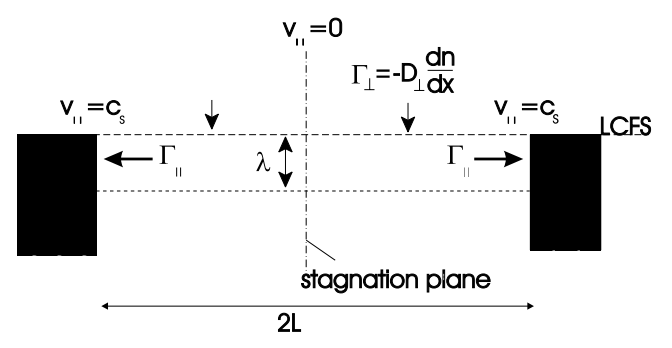


Figure 2: 2-d model of the SOL

q; the angle β in the poloidal plane between the field and the surface is given by the limiter shape or the orientation of the divertor plates. In torus geometry α varies along the poloidal coordinate depending on the aspect ration and the plasma pressure.

III. SCRAPE-OFF LAYER

Both concepts shown in fig. 1 are toroidally symmetric. This allows to discuss the main features by reducing the transport inside the SOL to a 2-dimensional problem: flow along the field line and diffusion in radial direction as shown in fig. 2.

The SOL begins at the last closed flux surface (LCFS). It is filled by a cross-field diffusion with flux density $\Gamma = -D_{\perp}\partial n/\partial x$. Because of the plasma sink at the end of the field lines a symmetric flow towards both ends develops. At the symmetry plane the parallel flow velocity v_{\parallel} must be zero (stagnation plane) and at both ends the flow velocity reaches sound speed, $v_{\parallel} = c_s$ (so called the "Bohm criterion"). With some simple estimates we may now characterize the main features of the SOL: a) SOL thickness, b) radial density variation and c) flow velocity profile along the field lines.

a) For a simple estimate we may relate the toroidal length of the flux tube (connection length 2L) and the SOL thickness λ to the average transport velocities v_{\parallel} and v_{\perp} according to

$$\frac{v_{\perp}}{v_{\parallel}} = \frac{\lambda}{L}.\tag{1}$$

For the average velocities we take $v_{\parallel} = 0.5c_s$ and $v_{\perp}n = D_{\perp}\partial n/\partial x$. With the characteristic length $\lambda = (1/n)\partial n/\partial x$ we obtain for Eq. 1

$$\frac{D_{\perp}/\lambda}{0.5c_s} = \frac{\lambda}{L}.$$
 (2)

From this relation we get the well known expression for the SOL thickness λ (i.e. the density decay length)

$$\lambda = \sqrt{\frac{D_{\perp}L}{0.5c_s}} \tag{3}$$

With typical values for an edge plasma $D_{\perp}=1m^2/s,\,T=50eV,\,$ and L=10 m we obtain $\lambda=30mm.$ This is a remarkably small value compared to the dimensions of a fusion reactor. As a consequence, the surface area wetted by the plasma reduces by roughly two orders of magnitude with respect to the total wall area, leading to unacceptable high heat loads. We will see later that this simple calculation even overestimates the SOL thickness, in particular close to the plasma facing components.

b) The radial variation f(x) of density inside the SOL can be derived from a simple 1d-calculation based on the conservation of mass along the flow channel z

$$\frac{\partial}{\partial x} D_{\perp} \frac{\partial n}{\partial x} = \frac{\partial}{\partial z} (n v_{\parallel}). \tag{4}$$

Assuming in a first step $D_{\perp} = const$ and $\partial n/\partial x = const$. along z as well as a constant r.h.s of Eq. 4 represented by $\partial/\partial z(nv_{\parallel}) = n/\tau_{\parallel}$ with a characteristic particle residence time in the SOL given by τ_{\parallel} (parallel transport to the target is the only plasma sink, no particle sources caused by ionisation of neutrals inside the SOL are considered) we obtain the solution of Eq. 4

$$n(x) = n(0) \exp(-x/\sqrt{D_{\perp}\tau_{\parallel}})$$
 (5)

The density shows an exponential decay inside the SOL with a characteristic length $\lambda = \sqrt{D_{\perp}\tau_{\parallel}}$ as given by Eq. 3, n(0) denotes the density at the LCFS. However, one has to be careful when using these equations, as particle sources inside the SOL and drifts will alter the result as discussed later on.

c) The variation along z under steady- state conditions can be deduced from the equations of particle and momentum conservation along the field lines under the assumption that the plasma temperature is constant along the field line (isothermal fluid model). Therefore, we have to prescribe the forces which drive the plasma flow towards the target. On a time scale of μs , electrons will rush ahead the ions as a consequence of their higher mobility and charge up the solid negatively. A thin sheath will form to shield the electrostatic potential with a characteristic length given by the so called Debye length

$$\lambda_D = \sqrt{\frac{\epsilon_0 k T_e}{ne^2}} \tag{6}$$

(the properties of this sheath will be discussed in section IV).

However, the shielding is imperfect because of the thermal motion of the plasma particles and a small electric field penetrates the plasma (pre-sheath). The electrons feel a retarding field. As their inertia is small, they obey a Boltzmann relation (V < 0)

$$n(z) = n(0) \exp(eV/kT_e). \tag{7}$$

The source term for the continuity equation along z is given by radial particle transport into the SOL (no ionisation inside the SOL)

$$\frac{\partial}{\partial z}(nv_{\parallel}) = S_p = -\frac{\partial}{\partial x}(D_{\perp}\frac{\partial n}{\partial x}) = \frac{D_{\perp}n}{\lambda^2}.$$
 (8)

For the ion momentum balance, we again neglect friction with neutrals (CX losses and ionisation) and represent the electric field with the help of the Boltzmann relation Eq. 7 yielding

$$m_i n v_{\parallel} \frac{\partial v_{\parallel}}{\partial z} = -k(T_e + T_i) \frac{\partial n}{\partial z} + m_i v_{\parallel} S_p$$
 (9)

with S_p as given by Eq. 8.

Defining a parallel Mach number $M_{\parallel} = v_{\parallel}/c_s$ and using the definition of the (isothermal) ion sound velocity $c_s = \sqrt{(k(T_e + T_i)/m_i)}$ we can now use Eqs. 8 and 9 to deduce two coupled equations which describe the variation of the density and the Mach number along z

$$\frac{\partial n}{\partial z} = -\frac{D_{\perp}}{c_s \lambda^2} \frac{2M_{\parallel}}{1 - M_{\parallel}^2} \tag{10}$$

$$\frac{\partial M_{\parallel}}{\partial z} = \frac{D_{\perp}}{c_s \lambda^2} \frac{1 + M_{\parallel}^2}{1 - M_{\parallel}^2} \tag{11}$$

The divergence of these two equations for $M_{\parallel}=\pm 1$ defines the boundary condition of the flow at the sheath entrance (the Bohm criterion as mentioned before). Combining Eqs. 10 and 11 we get

$$\frac{\partial n}{\partial M_{\parallel}} = -n \frac{2M_{\parallel}}{1 + M_{\parallel}^2} \tag{12}$$

which can be integrated analytically:

$$\frac{n}{n_0} = \frac{1}{1 + M_{\parallel}^2} \tag{13}$$

with n_0 the density in the stagnation plane where $M_{\parallel}(z=0)=0$. Therefore, the density drops from the stagnation point to the sheath entrance to half its value. As we assumed no variation of the particle source originating from cross field transport into the SOL and $|\partial n/\partial x|=n/\lambda=const.$, the SOL thickness λ reduces towards the target proportional to the density further aggravating the problem of the high target load as indicated before.

The equation describing the variation of the Mach number along z reads

$$M_{\parallel} - 2 \arctan M_{\parallel} = (\frac{\pi}{2} - 1) \frac{z}{L}$$
 (14)

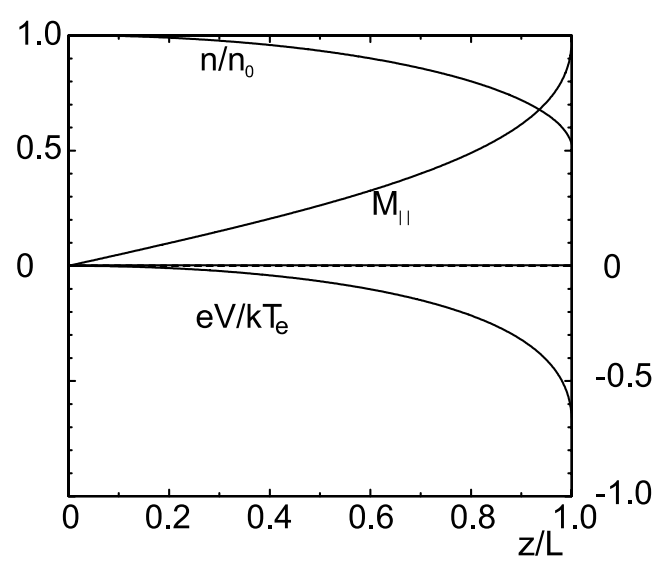


Figure 3: Variation of plasma density n normalized to n(0), parallel Mach number and normalised potential drop in the pre- sheath along the magnetic field from the stagnation plane z/L=0 to the sheath entrance z/L=1

Finally, combining Eq. 13 and 7 we get an equation for the potential in the pre-sheath

$$V(z) = -\frac{kT_e}{e} \ln{(1 + M_{\parallel}(z)^2)}$$
 (15)

Therefore, at $M_{\parallel}=1$ the total pre-sheath drop is given by $V\approx -0.69kT_e/e$.

Fig. 3 depicts the variation of the plasma density, the Mach number and the electric potential as given by Eqs. 13, 14 and 15, respectively, from the stagnation plane z/L=0 to the sheath entrance z/L=1.

Next we discuss briefly the influence of drift effects on the parallel particle transport in the SOL which have been identified as the cause of significant poloidal asymmetries in tokamaks ([7], [8], [9], [10], cf. also discussion in [3] and references therein).

The model for the parallel transport discussed before can be extended to include a perpendicular drift component caused by ExB drift, diamagnetic drift and ∇B and curvature drift. We decompose the drift motion into a radial and a binormal component $(\overrightarrow{e}_r \perp \overrightarrow{e}_\perp \perp \overrightarrow{e}_\parallel)$ which allows to express the poloidal velocity component v_θ as

$$v_{\theta} = v_{\parallel} \sin \alpha + v_{\perp} \cos \alpha \tag{16}$$

where α denotes the angle between the toroidal and poloidal magnetic field components as before $(\tan \alpha = B_{\theta}/B_{\phi})$.

As we will continue to investigate transport along the field line, we have to project the resulting poloidal velocity onto the parallel direction.

$$\tilde{v}_{\parallel} = v_{\parallel} + \frac{1}{\tan \alpha} v_{\perp}. \tag{17}$$

As a consequence Eqs. 10 and 11 are modified to

$$\frac{\partial n}{\partial z} = \frac{D_{\perp}}{c_s \lambda^2} \frac{2M_{\parallel} + M_{\perp}/\tan \alpha}{(M_{\parallel} + M_{\perp}/\tan \alpha)^2 - 1}$$
(18)

$$\frac{\partial M_{\parallel}}{\partial z} = \frac{D_{\perp}}{c_s \lambda^2} \frac{1 + (M_{\parallel} + M_{\perp}/\tan \alpha)^2}{1 - (M_{\parallel} + M_{\perp}/\tan \alpha)^2}$$
(19)

where M_{\perp} normalizes the perpendicular velocity to the sound speed. The boundary condition for the parallel Mach number at the sheath entrance reads

$$M_{\parallel}(z = \pm L) = \pm 1 - \frac{M_{\perp}}{\tan \alpha}.$$
 (20)

Consequently, the flow towards both sides of the limiter or to the two divertor plates shown in Fig. 1 is asymmetric, resulting in an asymmetric density distribution along the field line and in poloidal direction. Eq. 13 is replaced by

$$\frac{n}{n_0} = \frac{1}{1 + M_{\parallel}(M_{\parallel} + M_{\perp}/\tan\alpha)}.$$
 (21)

Within the simple model discussed above (still under the assumptions of no ionisations in the SOL) Fig. 4 illustrates the influence of a perpendicular Mach number $M_{\perp}=0.05$ on the parallel Mach number along the field line from the electron drift side of the ALT- II limiter in TEXTOR (located 45° below the outer midplane) to the ion drift side. The toroidal magnetic field and plasma current are anti- parallel under standard conditions in TEXTOR. In that case $M_{\parallel}>1$ on the ion drift side. The stagnation plane (as defined by $M_{\parallel}=0$) is considerably shifted away from the geometrical symmetry plane (located at z=0.5).

IV. THE SHEATH

Using the Bohm criterion discussed before (disregarding drifts) we can describe the ion flux density to the target as the parallel flux density at the sheath entrance (se) (neglecting additional sources in the very thin sheath)

$$\Gamma_{target}^{i} = n_{es}c_s = \frac{1}{2}n(0)\sqrt{\frac{k(T_i + T_e)}{m_i}}.$$
 (22)

To preserve ambipolarity the ion flux (for an ion charge Z=1) must balance the electron flux which is influenced by the sheath potential drop V_s . The electron distribution remains Maxwellian in the retarding electric field. Thus, the electron flux to the target reads

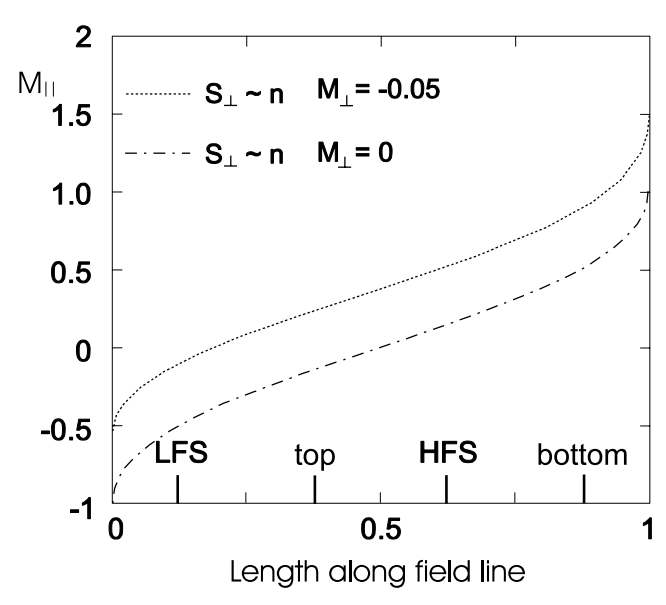


Figure 4: Influence of a perpendicular drift on the parallel Mach number $(\tan \alpha = 0.1, \text{ no ionisation in the SOL})$

$$\Gamma_{target}^{e} = \frac{1}{4} n_{es} \bar{c}_e = \frac{1}{4} n_{es} \exp\left(\frac{eV_s}{kT_e}\right) \sqrt{\frac{8kT_e}{\pi m_e}}.$$
 (23)

Equating 22 and 23 yields

$$\frac{eV_s}{kT_e} = 0.5 \ln \left(2\pi \frac{m_e}{m_i}\right) (1 + \frac{T_i}{T_e}). \tag{24}$$

Typical values for the ratio given above are about 3. To quantify the total potential drop between stagnation plane and target surface one has to add the presheath potential drop given in Eq. 15. Emission of electrons from the surface reduces the electrostatic potential. In some cases it can even lead to a breakdown of the sheath. The most important effect is the emission of secondary electrons, but also reflected electrons, photon induced emission and thermal emission play a role. In particular, above certain temperatures thermal emission can dominate and is considered to be one reason for the formation of so called hot spots [11].

The ions gain energy in the sheath (at the expense of the electrons which are cooled because only the fast part of the electron population can leave the plasma while the slower ones are repelled by the sheath potential). The impact energy of ions to the target, $E_{ion} = 2kT_i + 3ZkT_e$ with Z the charge of the ions, is significantly increased by the acceleration in the sheath, especially for highly charged impurity ions, leading to enhanced physical sputtering (cf. discussion in [2]).

The heat flux density of ions and electrons from the plasma onto the surface can be related to the particle flux densities leaving the plasma with the help of the so called "sheath transmission coefficients" defined as

$$\gamma_{i,e} = \frac{q_{i,e}}{kT_e\Gamma_{target}} \tag{25}$$

For electrons we get $\gamma_e \approx 2+3+0.5$ from the thermal, sheath and presheath contribution. The ions don't have a Maxwellian distribution, if they had, then $\gamma_i \approx 2.5 T_i/T_e + 0.5 + 0.5 T_i/T_e$. Numerical simulations allowing for non-Maxwellian ion distributions give somewhat smaller results $\gamma_i \approx 2-3$. The total sheath transmission coefficient is then around $\gamma=8$. The heat flux density to the target can be expressed as

$$q_{target} = \gamma n_{es} c_s k T_e = \frac{1}{2} n(0) \sqrt{\frac{k(T_i + T_e)}{m_i}} k T_e. \quad (26)$$

The magnetic field \overrightarrow{B} has no influence on the sheath description as long as the surfaces are orthogonal to \overrightarrow{B} . In practice, however, surfaces are tilted to spread the power onto the target. The effect of oblique target surfaces on the sheath is discussed in [6].

V. PLASMA PARAMETERS AT THE SURFACES

The flux densities of heat and particles to the limiters / target plates of divertors are determined by the local plasma parameters n and T (we assume $T_e = T_i = T$ for the following) as described in Eqs. 22 and 26. These equations allow to derive local plasma parameters from independent measurements of q and Γ (e.g. via thermography and spectroscopy). We may now estimate how global parameters like the total heating power, the total number of plasma particles and confinement times can influence n and T. From 22 and 26 we deduce the relations

$$T \propto q/\Gamma$$
 (27)

$$n \propto \Gamma^{3/2}/q^{1/2} \tag{28}$$

For example increasing q by stronger heating would lead to an increase of T but also a drop of n, provided the particle fluxes are kept constant. Since with additional heating normally also the particle flux increases (caused by a confinement degradation for both energy and particles), we observe also an increase of n. In contrast, edge cooling by impurity radiation may lead to a decrease of q with the consequence of lower T. With extreme cooling at high densities and low power the particle confinement can increase (Γ decreases) such that also n drops significantly (detached plasma).

Owing to re-ionisation of recycling neutrals inside the SOL a significant flux amplification may develop. In this case the simple model described in section III

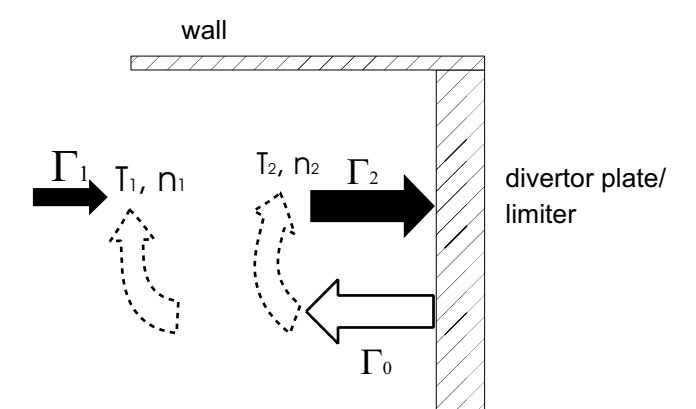


Figure 5: Flux inside a divertor or in the vicinity of a limiter: neutral flux Γ_0 , ion fluxes Γ_1 and Γ_2 , local temperatures T and densities "upstream" (1) and close to the target (2)

is no longer valid and we have to distinguish the fluxes (heat q_1 and particles Γ_1) entering the recycling zone ("upstream") from those just at the surface of the divertor plate or limiter Γ_2 . This situation is illustrated in Fig. 5

Flux amplification occurs if a considerable fraction of the recycling neutral flux Γ_0 is re- ionized in the SOL close to the target and contributes to the ion flow such that $\Gamma_2 > \Gamma_1$. We may define the flux amplification factor as $F = \Gamma_2/\Gamma_1$. Introducing this into Eqs. 27 and 28 we obtain the following relations for the temperature and density close to the target

$$T_2 \propto q/(F\Gamma_1)$$
 (29)

$$n_2 \propto (F\Gamma_1)^{3/2}/q^{1/2}$$
. (30)

Flux amplification (F > 1) increases the density at the target $(\propto F^{3/2})$ and decreases the the temperature $(\propto F^{-1})$). A temperature gradient along the field lines has to develop causing heat transport via conduction, because the heat sources of the plasma remain in the plasma bulk even if all particles are ionized in the SOL. In general, such a situation with large fractions of ionization in the SOL and significant temperature gradients along the field lines only develop in divertor geometry where the shielding of the confined plasma from the recycling neutrals is much more effective ("high recycling regime").

The main effect of the flux amplification is a reduction of sputtering processes owing to the lower plasma temperature while the total heat flux to the target is not changed. In these considerations it has been assumed that all heat and particle fluxes finally reach the limiter/ divertor plate by convection. However, charge

exchange (CX) processes between plasma ions and neutrals may redirect a significant part of the fluxes to the surrounding wall. This fraction is limited to about 25% of the total flux if the the CX processes occur mainly lose to the target (region 2). Higher fractions are possible if the region of CX is extended to hotter parts of the plasma (region 1). In that case the plasma pressure is no longer constant along the field lines because of the momentum losses by the ion- neutral friction. Furthermore, also impurity radiation inside the SOL may contribute to a distribution of power to larger areas. Both, momentum and power reduction along the field line lead to a so called detachment of the plasma from the target.

We can quantify the effects in the complex SOL of a divertor using a simple analytical model (the so called "two point model", cf. [3], chapters 4 and 5). This model relates the conditions upstream of the target (position 1) to those at the target (position 2) in the case where the fraction f_{cond} of the power is conducted along the parallel temperature gradient as

$$q_{||,cond} = f_{cond} P_{SOL} / A_{q||} = -\kappa_0 T^{5/2} dT / dz,$$
 (31)

where $\kappa_0 \approx 2000$ for electrons and $\kappa_0 \approx 60$ for ions $(q \text{ is given in } W/m^2 \text{ and } T \text{ in eV}, P_{SOL}$ is the power flow into the SOL and $A_{q||}$ the total cross-sectional area of the SOL for power flow perpendicular to \overrightarrow{B} (no additional power flow into the SOL between position 1 and 2). We include possible volumetric power sinks characterised by the factor $f_{loss} > 0$ in the balance between power flux into the SOL and power flux at the sheath entrance as

$$(1 - f_{loss})P_{SOL}/A_{q||} = \gamma n_2 c_s k T_2 \tag{32}$$

(cf. Eq. 26 in section IV).

We further introduce a factor $f_{fric} < 1$ into the pressure balance to take pressure losses because of momentum sinks and friction into account

$$n_1 T_1 f_{fric} = 2n_2 T_2.$$
 (33)

Integrating Eq. 31 over the distance L between the upstream region 1 and the target region 2 leads to

$$T_2^{7/2} = T_1^{7/2} - \frac{7 P_{SOL} L}{2 A_{a||} \kappa_0} f_{cond}.$$
 (34)

Because $T_2^{7/2} \ll T_1^{7/2}$ as soon as a temperature gradient exists the upstream temperature is given as

$$T_1 = \left(\frac{7 P_{SOL} L}{2 A_{q||} \kappa_0} f_{cond}\right)^{2/7} \tag{35}$$

showing a very weak dependence on all parameters.

If we now take n_1 and $P_{SOL}/A_{q||}$ as given, we can derive from Eqs. 32, 33 and 35 an expression for the temperature at the target

$$T_{2} = \frac{m_{i}}{2e} \frac{4(P_{SOL}/A_{q||})^{2} \left(\frac{7}{2} \frac{P_{SOL}L}{A_{q||}\kappa_{0}}\right)^{-4/7}}{\gamma^{2}e^{2}n_{1}^{2}} \cdot \frac{(1 - f_{loss})^{2}}{f_{fric}^{2} f_{cond}^{4/7}}.$$
(36)

Correspondingly we get for the density n_2 at the target

$$n_2 = \frac{n_1^3}{(P_{SOL}/A_{q||})^2} \left(\frac{7}{2} \frac{P_{SOL}L}{A_{q||}\kappa_0}\right)^{6/7} \frac{\gamma e^2}{2m_i} \cdot \frac{f_{fric}^3 f_{cond}^{6/7}}{(1 - f_{loss})^2}.$$
(37)

High upstream densities n_1 are very efficient to realise a cold and dense high recycling divertor. We further note that the plasma conditions at the target depend very sensitively on the loss parameters f_{loss} , f_{cond} and f_{fric} , which can only be obtained from sophisticated modelling. As a result, divertor regimes with high recycling or detachement and also regimes with a radiating divertor can be quite unstable and difficult to control. Nevertheless, much effort is spent to explore these regimes because of their potential to reduce the problem of power load to the target (see, e.g. discussion in [3] and references therein).

VI. NEUTRAL PARTICLE TRANSPORT

Hydrogen and impurity neutrals are released from the plasma facing components and penetrate into the edge plasma. Owing to the different release mechanisms as discussed in [2] we observe also different particle velocities. This has an important impact on the edge plasma.

Hydrogen may be released as a molecule H_2 or an atom H_0 . It has been found that in the recycling process the probability for molecule formation depends on the surface temperature, which determines the residence time in the surface. At low temperatures mainly molecules are desorbed while above about $T_s = 1200K$ the majority of particles is released as atoms [12] [13].

Some processes involved with the penetration of H_2 are illustrated in Fig. 6. Because of electron impact the molecule dissociates. Various dissociation channels compete, with cross sections depending on T_e . Some of them are given in table 1 together with the rate coefficients for $T_e = 50$ eV.

The reaction no.1, also illustrated in Fig. 6, is only dominant at or below $T_e = 10eV$, whereas at higher T_e the molecule is first ionized and then dissociated (reactions no.3 and no.4), as is obvious from the rate coefficients $\langle \sigma v \rangle_{dis}$ [14]. The atoms resulting from the

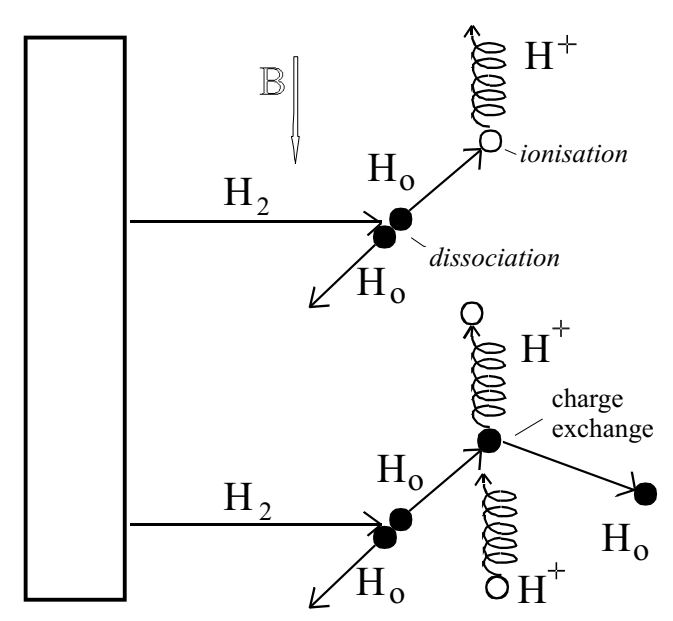


Figure 6: Molecule dissociation and charge exchange processes at the plasma boundary (solid circles: atoms, open circles: ions)

no.	dissociation reaction	$<\sigma v>_{dis}/m^3/s$
1	$H_2 \rightarrow H_0 + H_0$	$6 \cdot 10^{-15}$
2	$H_2 \rightarrow H_0 + H^+$	$2 \cdot 10^{-15}$
3	$H_2 ightarrow H_2^+$	$4 \cdot 10^{-14}$
4	$H_2^+ \to H_0^- + H^+$	$3 \cdot 10^{-13}$
5	$H_2^+ \rightarrow H^+ + H^+$	$6 \cdot 10^{-15}$

Table 1: Dissociation reactions of hydrogen molecules and molecular ions[14].

dissociation of molecules in ground state gain energies in the range of 2.2eV. Surprisingly, average energies significantly lower than these (0.5eV) have been measured in the vicinity of a limiter [15] [16]. It is assumed that this is caused by vibrationally excited molecules.

The probability that an atom has at least one charge exchange (CX) reaction before it is ionised is rather high because the rate coefficients for ionisation $<\sigma v>_i$ and CX $<\sigma v>_{CX}$ are similar as is shown in the table 2 [14].

Using the atomic and molecular data the transport of neutral particles can be modeled with a rather high accuracy even for complicated 3d-geometries [17].

The velocity of impurity atoms produced depends on their release mechanisms. The fastest particles are

$T_e = T_i$	10		eV
$<\sigma v>_i$ $<\sigma v>_{CX}$	$7 \cdot 10^{-15}$	$3 \cdot 10^{-14}$	$m^3 s^{-1}$
$<\sigma v>_{CX}$	$2\cdot 10^{-14}$	$5 \cdot 10^{-14}$	$m^3 s^{-1}$

Table 2: Rate coefficients for ionisation and charge exchange [14].

reflected impurities (impurity ions from the plasma, neutralised and re-emitted). Among the erosion mechanisms, sputtering generates particles in the range of 5 eV. Atoms coming from molecules gain their velocity from the dissociation energy. Sublimated or evaporated atoms have only thermal energy, thus represent the slowest particles with the least impact on the edge plasma (cf. discussion in [2]).

Recombination processes are generally not important unless the plasma is very cold as in detached divertors, since in most cases the recombination times of ions are much longer than the average residence time of the particles in the plasma.

The ionisation time of an atom can be calculated from the rate coefficient for ionisation $\langle \sigma v \rangle_i$ (T_e) and the local electron density n_e . The time derivative of the neutral density n_0 owing to ionisation is then given by

$$\frac{\partial n_0}{\partial t} = -n_e n_0 < \sigma v >_i \tag{38}$$

leading to an exponential decay of the atom density

$$n_0(t) = n_0(t=0) \exp(-\frac{t}{\tau_i}).$$
 (39)

The ionisation time τ_i is given by

$$\tau_i = \frac{1}{n_e < \sigma v >_i} \tag{40}$$

The penetration of neutral particles into a homogeneous plasma having a velocity v_0 is given by the ionisation length

$$\lambda_i = \frac{v_0}{n_e < \sigma v >_i} \tag{41}$$

In the presence of a radial profile of both the electron density and temperature the description of the ionisation length can be generalised to

$$\int_0^{\lambda_i} \frac{n_e(r) \langle \sigma v \rangle_i (T_e(r))}{v_0} dr = 1$$
 (42)

We can define the ion source distribution Q(r), which is given under steady- state conditions as

$$Q(r) = -\frac{\partial \Gamma_0}{\partial r} = n_0(r)n_e(r) < \sigma v >_i (T_e(r))$$
 (43)

Here, $\Gamma_0 = n_0 v_0$ is the neutral flux density under the simplifying assumption of a mono-energetic neutral velocity distribution. The ionisation length λ_i can be used to characterise the radial extent of the ion source distribution. As a consequence the impact of neutrals on the edge plasma is characterised both by their velocities as determined by the specific release mechanism and the edge plasma parameters n_e and T_e . As stated before, for hydrogen atoms charge exchange processes are important in addition. This gives rise to a diffusion process of the atoms. The penetration depth is given by the geometric mean of the ionisation length λ_i as given by Eq. 41 and the mean free path for the CX process λ_{CX} [18] using for both (!) the thermal ion velocity $v_{th} = \sqrt{kT_i/m_i}$

$$\lambda_{pen} = \frac{v_{th}}{n_e \sqrt{\langle \sigma v \rangle_{CX} \langle \sigma v \rangle_i}}.$$
 (44)

REFERENCES

- U. Samm, "Radiation Phenomena at the Edge", these proceedings.
- 2. V. Philipps, "Plasma- Wall Interaction", these proceedings.
- 3. P.C. Stangeby, "The Plasma Boundary of Magnetic Fusion Devices", Plasma Physics Series, IoP Publishing Ltd, Bristol, UK (2000).
- 4. S. Wiesen, "Helium Removal and Recycling", these proceedings.
- D. Reiter, G.H. Wolf and H. Kever, Nucl. Fusion 30 (10) 2141 (1990).
- 6. K.H. Finken, "Edge Physics, Divertors, Pump Limiters", these proceedings.
- 7. H. Gerhauser and H.A. Claassen, J. Nucl. Mater. **176-177**, 721 (1990).
- 8. M. Baelmans, D. Reiter and R.R. Weynants, Contrib. Plasma Phys., **36** 117 (1996).
- 9. M. Lehnen, M. Brix, U. Samm, B. Schweer, B. Unterberg and the TEXTOR- team, Nucl. Fusion 43 168. (2003).
- M. Lehnen, M. Brix, H. Gerhauser, B. Schweer and R. Zagorski, J. Nucl. Mater. 290-293 (3) 663 (2001).
- 11. V. Philipps et al., Nucl. Fusion **33** (6), 953 (1993).
- P. Franzen and E. Vietzke, J. Vac. Sci. Technol. A12 820 (1994).
- A. Pospieszczyk et al., J. Nucl. Mater. 266-269 138 (1999).
- M.F.A. Harrison in "Applied Atomic Collision Physics", Vol.2, Academic Press 1984, Eds. C.F. Barmett and M.F.A. Harrison (1984).
- J.D. Hey et al., Contrib. Plasma Phys. 36 583 (1996).
- A. Pospieszczyk and Ph. Mertens, J. Nucl. Mater. 266-269 884 (1999).
- 17. D. Reiter, J. Nucl. Mater. **196-198** 80 (1992).
- 18. B. Lehnert, Nucl. Fusion 8 173 (1968).